RPL13 Variants Cause Spondyloepimetaphyseal Dysplasia with Severe Short Stature

Cedric Le Caignec,[1,21] Benjamin Ory,[2,21] François Lamoureux,[2,21] Marie-Francoise O'Donohue,[3] Emilien Orgebin,[2] Pierre Lindenbaum,[4] Stéphane Téletchéa,[5] Manon Saby,[6] Anna Hurst,[7] Katherine Nelson,[7] Shawn R. Gilbert,[8] Yael Wilnai,[9] Leonid Zeitlin,[10] Eitan Segev,[10] Robel Tesfaye,[2] Mathilde Nizon,[1] Benjamin Cogne,[1] Stéphane Bezieau,[1] Loic Geoffroy,[11] Antoine Hamel,[11] Emmanuelle Mayrargue,[11] Benoît de Courtivron,[12] Aliette Decock-Giraudaud,[13] Céline Charrier,[2] Olivier Pichon,[1] Christelle Retière,[14,15] Richard Redon,[4] Alexander Pepler,[16] Kirsty McWalter,[17] Lydie Da Costa,[6,18] Annick Toutain,[19] Pierre-Emmanuel Gleizes,[3,22] Marc Baud'huin,[20,22,*] and Bertrand Isidor[1,22,*]

Variants in genes encoding ribosomal proteins have thus far been associated with Diamond-Blackfan anemia, a rare inherited bone marrow failure, and isolated congenital asplenia. Here, we report one *de novo* missense variant and three *de novo* splice variants in *RPL13*, which encodes ribosomal protein RPL13 (also called eL13), in four unrelated individuals with a rare bone dysplasia causing severe short stature. The three splice variants (c.477+1G>T, c.477+1G>A, and c.477+2 T>C) result in partial intron retention, which leads to an 18-amino acid insertion. In contrast to observations from Diamond-Blackfan anemia, we detected no evidence of significant pre-rRNA processing disturbance in cells derived from two affected individuals. Consistently, we showed that the insertion-containing protein is stably expressed and incorporated into 60S subunits similar to the wild-type protein. Erythroid proliferation in culture and ribosome profile on sucrose gradient are modified, suggesting a change in translation dynamics. We also provide evidence that RPL13 is present at high levels in chondrocytes and osteoblasts in mouse growth plates. Taken together, we show that the identified *RPL13* variants cause a human ribosomopathy defined by a rare skeletal dysplasia, and we highlight the role of this ribosomal protein in bone development.

Because ribosomes translate mRNAs, they are universally responsible for the quality and quantity of proteins in all cells. Their production is highly regulated by many cellular processes, including growth, proliferation, and differentiation.[1] Assembly of the 80 ribosomal proteins (RPs) and four ribosomal RNAs (rRNAs) that form the two ribosomal subunits involve hundreds of ribosome biogenesis factors (RBFs). Variants in genes encoding RPs or RBFs have been linked to a growing class of genetic conditions called ribosomopathies. These conditions often include inherited bone marrow failure (IMBF), but various other tissues are affected, such as bones, spleen, pancreas, and heart.[2] Variants in genes encoding RPs have been described in a restricted set of congenital pathologies: Diamond-Blackfan anemia (DBA; >20 different RP genes [MIM: 105650]), isolated congenital asplenia (ICA [MIM: 271400], *RPSA*),[3] an autism syndrome (MIM: 617412) (*RPS23*),[4] and predisposition to hereditary nonpolyposis colorectal carcinoma (MIM: 120435) (*RPS20*).[5] DBA is described as a pure red-cell aplasia, while ICA is characterized by absence of the spleen without any other developmental defect. How variants in ubiquitously expressed genes can yield such tissue-specific phenotypes remains an open question.

We report four unrelated individuals affected by a severe spondyloepimetaphyseal dysplasia (SEMD) which was first described in 2013.[6] The clinical and radiological abnormalities observed in these individuals are summarized in Table S1. Individuals 1 and 2 were reported as having a rare form of SEMD[6] which is similar to SEMD matrilin-3 related (MIM: 608728) and SEMD Strudwick type (MIM: 184250). All individuals shared common major features: normal birth length, early postnatal growth deficiency, severe short stature, and genu varum. Skeletal radiographies showed platyspondyly and severe epiphyseal

[1]CHU Nantes, Service de génétique médicale, F-44000 Nantes, France; [2]Nantes Université, INSERM, Bone sarcomas and remodeling of calcified tissues, UMR 1238, F-44000 Nantes, France; [3]Laboratoire de Biologie Moléculaire Eucaryote, Centre de Biologie Intégrative (CBI), Université de Toulouse, UPS, CNRS, 31062 Toulouse, France; [4]L'institut du thorax, INSERM, CNRS, Université de Nantes, F-44000 Nantes, France; [5]Nantes Université, CNRS, Unité Fonctionnalité et Ingénierie des Protéines (UFIP), UMR CNRS 6286, F-44000 Nantes, France; [6]INSERM U1149/ERL 8252, Inflammation Research Center, 75018 Paris, France; [7]Department of Genetics, University of Alabama at Birmingham, Birmingham, AL 35233, USA; [8]Children's of Alabama, Department of Orthopaedic Surgery, University of Alabama at Birmingham, Birmingham, AL 35233, USA; [9]Genetic Institute, Tel Aviv Sourasky Medical Center, Tel Aviv 6423906, Israel; [10]Pediatric Orthopedic Department, Dana-Dwek Children's Hospital, Tel Aviv Sourasky Medical Center, Tel Aviv 6423906, Israel; [11]Service d'Orthopédie Pédiatrique, CHU de Nantes, F-44000 Nantes, France; [12]Service de Chirurgie Orthopédique Pédiatrique, CHU de Tours, 37044 Tours, France; [13]CRB/Tumorothèque, CHU de Tours, 37044 Tours, France; [14]Etablissement Français du Sang, F-44000 Nantes, France; [15]CRCINA, INSERM, CNRS, Université d'Angers, Université de Nantes, F-44000 Nantes, France; [16]Center for Genomics and Transcriptomics and Praxis für Humangenetik Tübingen, 72076 Tübingen, Germany; [17]GeneDx, Gaithersburg, MD 20877, USA; [18]AP-HP, Service d'Hématologie Biologique, Hôpital R. Debré, Université Paris 7 Denis Diderot, Sorbonne Paris Cité, 75019 Paris, France; [19]Service de Génétique, CHU de Tours, 37044 Tours, France; [20]Nantes Université, CHU Nantes, INSERM, Bone sarcomas and remodeling of calcified tissues, UMR 1238, F-44000 Nantes, France
[21]These authors contributed equally to this work
[22]These authors contributed equally to this work
*Correspondence: marc.baudhuin@univ-nantes.fr (M.B.), bertrand.isidor@chu-nantes.fr (B.I.)
https://doi.org/10.1016/j.ajhg.2019.09.024.

Table 1. Clinical and Radiological Observation in Affected Individuals

-	P1	P2	P3	P4
RPL13 variant (NM_000977.3)	c.477+1G>T	c.477+2T>C	c.477+1G>A	c.548G>C
DNA (RefSeq accession number: NC_000016.9, ref GRCh37.p13)	g.89628800 G>T	g.89628801 T>C	g.89628800 G>A	g.89629362 G>C
Protein (RefSeq: NP_000968.2)	p.Asn159_Val160ins18	p.Asn159_Val160ins18	p.Asn159_Val160ins18	p.Arg183Pro
ExAC/gnomAD frequency	absent	absent	absent	absent
Mode of inheritance	*de novo*	*de novo*	*de novo*	*de novo*
Method of variant detection	ES trio	ES trio	ES trio	ES trio
Gender	M	M	M	F
Skeletal Findings				
Prenatal length < 2SD	-	-	-	-
Short stature	+++	+++	+++	+
Genu varum	+	+	+	+
Scoliosis	-	+	-	-
Hyperlaxity	-	-	-	-
Extraskeletal Findings				
Cone-rod dystrophy	-	-	-	-
Myopia	-	-	-	-
Deafness	-	-	-	-
Anemia	-	-	-	-
Radiological Findings				
Platyspondyly	+	+	+	+
Bowed femora			+	+
Shortened long bones	+	+	+	+
Metaphyseal involvement	+	+	+	+
Lower limbs epiphyseal changes	+	+	+	+
Upper limbs epiphyseal changes	-	-	+	-
Pelvis				
Coxa vara	+	+	+	+
Hands				
Short phalanges	-	-	-	-

and metaphyseal changes in lower limbs. None of the individuals presented any episodes of anemia, and they all had a normal blood count at last follow-up.

Through trio exome sequencing of individuals P1 and P2 and their parents, we identified two *de novo* intronic single-nucleotide variants in *RPL13* (NM_000977.3, [MIM: 113703]): c.477+1G>T in individual P1 and c.477+2T>C in individual P2 (Table 1). These variants are absent in public variant databases (dbSNP138, 1000 Genomes, NHLBI GO Exome Sequencing Project, gnomAD). Through GeneMatcher,[7] we subsequently identified two additional individuals (P3 and P4) with *RPL13* variants (c.477+1G>A and c.548G>C [p.Arg183Pro]); we also identified these variants through the use of trio-based exome sequencing. Both individuals were followed for short stature with SEMD (Figure 1A).

To confirm the pathological effect of the c.477+1G>T and c.477+2T>C variants, we performed RT-PCR on RNA isolated from peripheral blood samples from individuals P1 and P2. cDNA was used as a template for PCR using primers (Table 1). Agarose gel electrophoresis using cDNA showed an aberrant longer fragment amplified in both individuals, in addition to the normal 695 bp amplification product observed with control cDNA (Figure 1B, left panel).

Sanger sequencing of the aberrant amplified products revealed the presence of the first 54 bp of intron 5 (Figure 1C). These results confirmed that the intronic

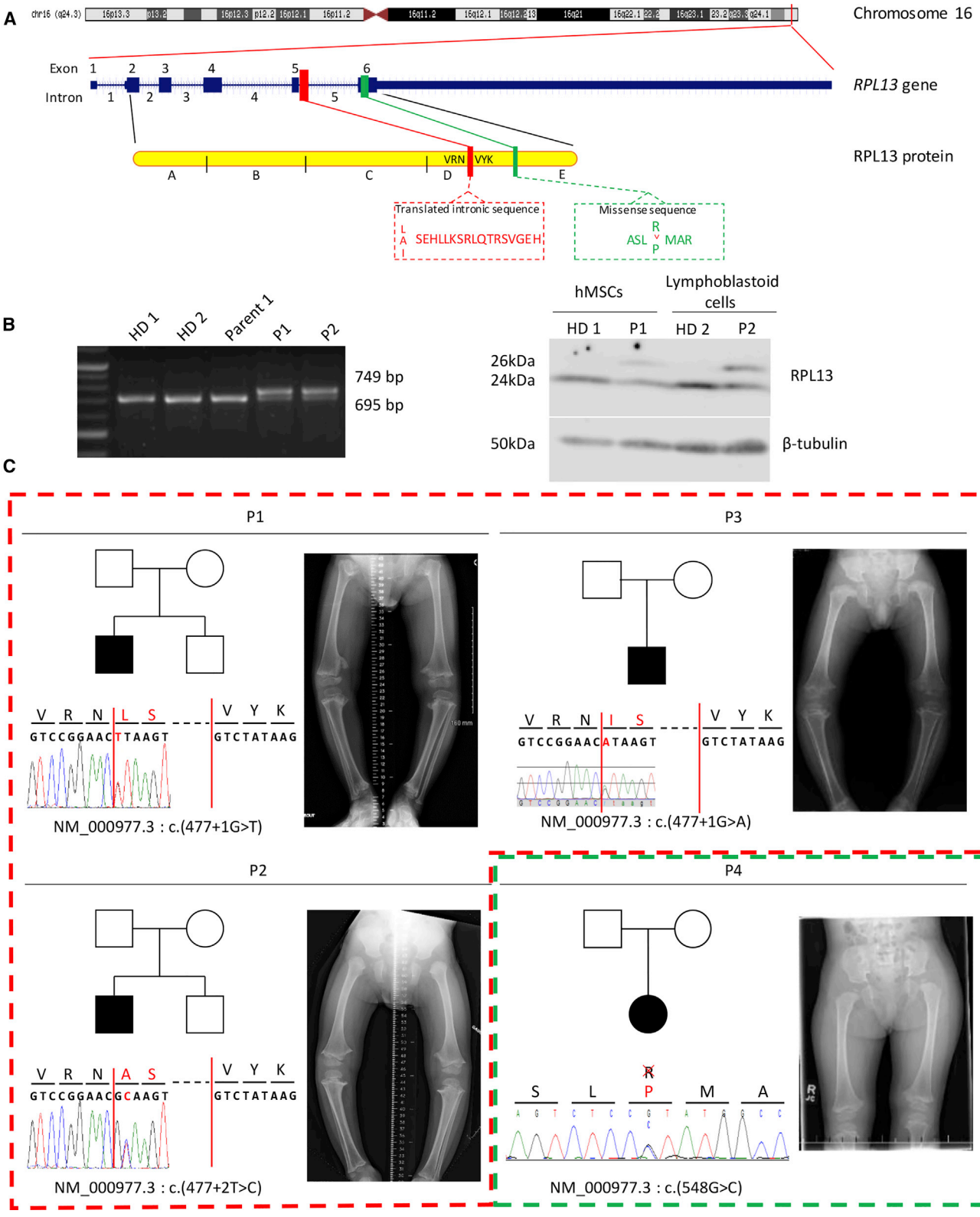

Figure 1. Mapping and Localization of the RPL13 (eL13) Variants Observed in Four Individuals
(A) Schematic representation of the gene RPL13 located in 16q24.3 region and its protein with the site of variants in the intron 5.
(B) Agarose gel electrophoresis of RT-PCR products of RPL13 mRNA from two healthy donors, one parent, P1, and P2 (left panel). Western blot analysis of cell lysates from MSCs or lymphoblastoid cells from healthy donors (HD), P1, and P2 illustrating the presence of the variant protein RPL13, 2kDa larger than the wild type protein. β-tubulin was used as loading control (right panel).
(C) Pedigree drawings, intragenic variants of RPL13 revealed by Sanger and X-Rays photographs of individuals at the ages (respectively) of 4 years and 4 months (P1), 3 years and 4 months (P2), 4 years (P3), and 2 years and 10 months (P4) showing shortened long bones, bowed femora with metaphyseal enlargement, and irregularities.

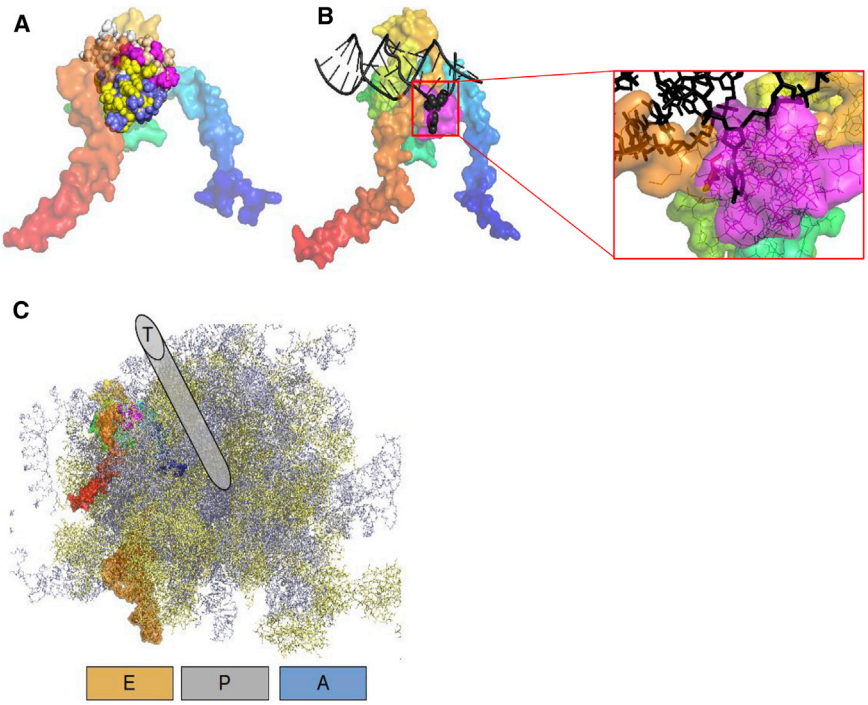

Figure 2. Structural Consequences of the Polypeptide Insertion on RPL13 and Ribosomal Architecture

(A) The U-shaped RPL13 structure in surface representation is colored from the N-terminal in blue to the C-terminal in red. The polypeptide insertion introduce a compact patch displayed in sphere representation (model 1, magenta; model 2, yellow; model 3, tan; model 4, white; model 5, blue).

(B) The insertion for model 1 (magenta surface) would induce a steric clash with Adenine 509 (in sphere representation) of the 28S RNA (black) in its ES7L region.

(C) General organization of the ribosome including the variant RPL13 protein. The 40S subunit is removed for clarity, 60S proteins are indicated in yellow, 60S RNAs are indicated in gray. Letters A, P, and E allow approximatively location of the aminacyl, the peptidyl, and the exit sites. The tRNA found in the deposited structure at the exit site is displayed in orange surface. The polypeptidic exit tunnel (T) is indicated above the picture although its exact location is more buried in the ribosome structure.

missense variants abolish the natural donor splice-site of intron 5 and demonstrated that a cryptic new donor splice located in intron 5 of *RPL13* was utilized in individuals P1 and P2. This leads to an abnormal mRNA containing 54 bp of intron 5. Translation of this abnormal mRNA is expected to encode a 229-amino-acid protein containing the 18 supplementary amino acids. The fourth c.548G>C variant was confirmed by Sanger sequencing and was *de novo*. It leads to the substitution of arginine 183 by a proline, which is expected to break the long alpha-helix present at the C terminus of the protein. The arginine 183 is highly conserved throughout species (PhastCons score 1, Mutation Taster[8]). This variant is also absent from all genomic databases and is predicted to be pathogenic (score 0.966 [PolyPhen[9]], PHRED score 26.0 [CADD[10]], score 106 [Mutation Taster]).

At the protein level, western blot analysis carried out on protein lysates from mesenchymal stem cells (MSCs, individual P1) and from lymphoblastoid cells (individual P2) confirmed RT-PCR data. Two bands (24kDa and 26kDa) were detected for the two individuals, and only one band was detected in control cells (Figure 1B, right panel). The two bands differed by 2kDa, corresponding to an 18-residue peptide coded by the first 54 bp of intron 5.

To assess the putative consequences of RPL13 variants on the ribosome structure, the 18-residue-long (individuals P1, P2, and P3) peptide was inserted into the RPL13 sequence and submitted to I-TASSER for structure prediction. The first model obtained had a TM-Score of 0.44,[11] which is indicative of a high confidence in the models. All five predicted models are very similar, with a root-mean-square deviation (RMSD) between them less than 2 Å to the native RPL13 fold. The 18-residue-long polypeptide addition is modeled as a compact structure conserving the U-shaped RPL architecture (Figure 2A). In the human ribosome structure, RPL13 is in contact with Expansion Segment 7L (ES7L) of the 28S RNA around positions 500–530 (complementary strand: 630–660). A direct interaction between adenine 509 and RPL13 tyrosine 161 is clearly observed in the deposited 4V6X structure, with the adenine extruded from the double-stranded DNA. The additional polypeptide insertion, as modeled in our study, would introduce steric clashes with the DNA at that position, thus preventing this specific interaction (Figures 2B and 2C). This polypeptide patch seems nevertheless compatible with a merely intact ribosome structure because RPL13 presents an extended contact zone at the surface of the ribosome, close to the tRNA exit site (Figure 2D).

To investigate the functional consequences of RPL13 variants on ribosome biogenesis, we first assessed their impact on pre-rRNA processing by comparison with cells depleted of RPL13. As shown in Figure 3A, knockdown of RPL13 with siRNAs in HeLa cells severely affected the pre-rRNA pattern detected by northern blot. The most conspicuous effect was a defect in pre-rRNA cleavage at site 2 in ITS1, as revealed by the accumulation of 41S pre-rRNA relative to the 30S and 21S pre-rRNAs, and the high levels of 36S and 36S-C pre-rRNAs. We also noticed a drop of the levels of 12S pre-rRNA relative to its precursor, the 32S pre-rRNA (Figures 3A). A similar phenotype was observed in a control lymphoblastoid cell line treated with these siRNAs (Figure S1). When analyzed through the use of northern blot, total RNAs

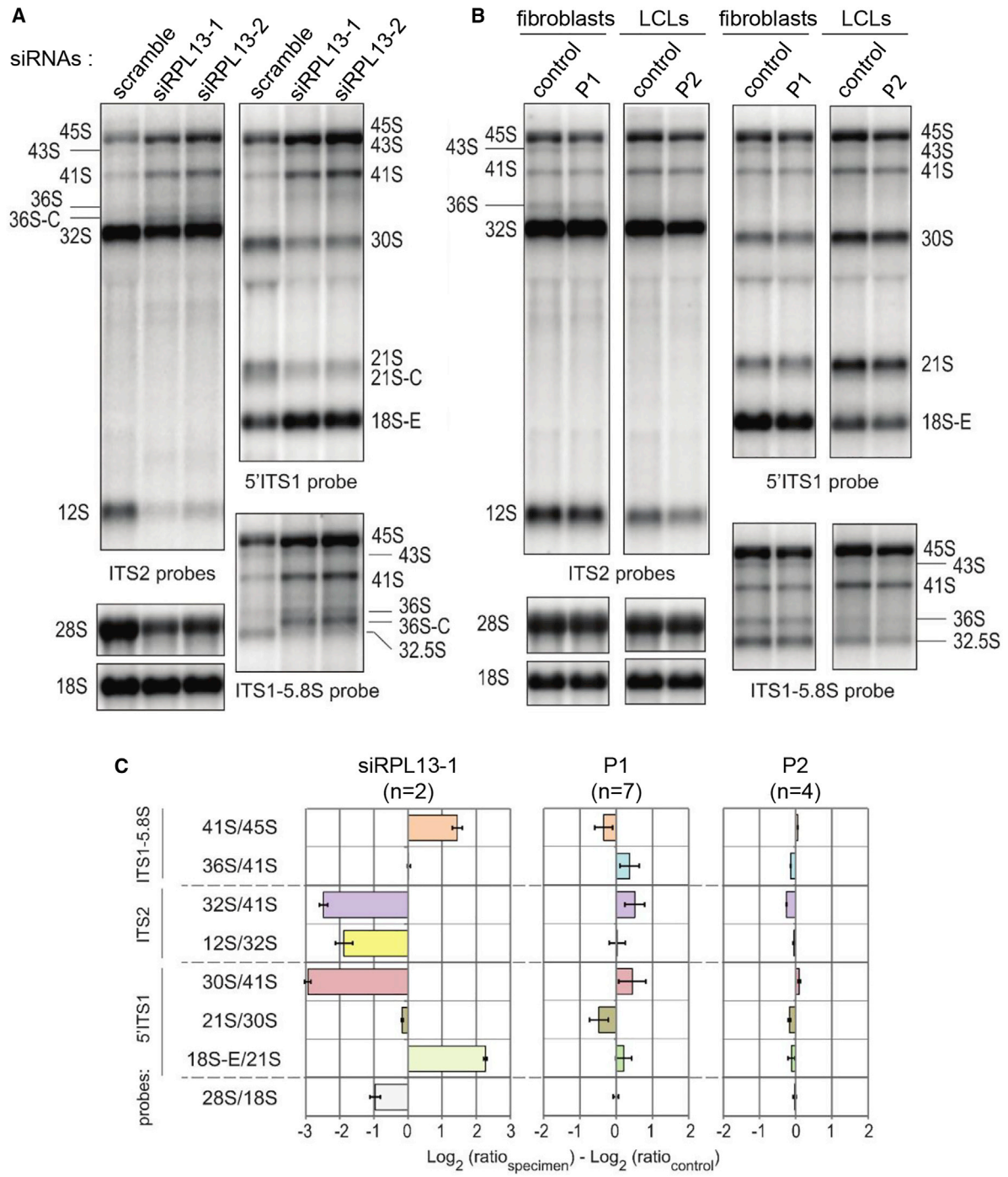

Figure 3. Consequence of Mutant RPL13 on Pre-rRNA Processing

(A) Northern blot analysis of pre-RNAs in HeLa cells treated with RPL13 siRNAs. The 5′ITS1 and the ITS2 probes detect the precursors to the 40S and 60S subunit RNAs, respectively. The ITS1-5.8S probe evidences accumulation of 36S and 36S-C precursors, indicative of a defect in cleavage at site 2.

(B) Northern blot analysis of pre-rRNAs from fibroblasts of individual P1, lymphoblastoid cells of individual P2, and healthy donors with the same probes as in (A).

(C) Quantification of changes in the pre-rRNA pattern in (A) and (B) by ratio analysis of multiple precursors (RAMP)(27), expressed as variations relative to the respective controls (number of replicate are stated in the figure). The analysis shows no significant variation in individual cells, unlike in RPL13 siRNA-treated cells.

from cells established from individuals P1 and P2 did not show such an abnormal pre-rRNA pattern, indicating that the RPL13 variants do not affect pre-rRNA maturation like a null mutant does (Figures 3B and 3C). Consistent with the lack of impact on pre-rRNA processing, a ribosome profile on a sucrose gradient in lymphoblastoid cells from individual P2 showed a normal ratio of free 40S to 60S subunits compared to the control (Figures

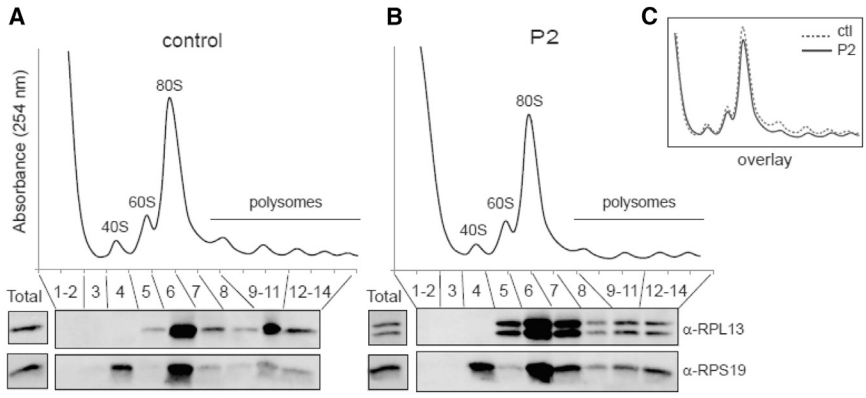

Figure 4. Incorporation of Variant RPL13 in Large Ribosomal Subunits

(A and B) Polysome profiles of lymphoblastoid cells from a healthy control (A) and from individual P2 (B) displaying free small ribosomal subunits (40S peak) and free large ribosomal subunits (60S peak). Monosomes (80S peak) and polysomes correspond to mRNAs bearing single ribosomes or several ribosomes, respectively. Western blot analyses probed with anti-RPL13 and anti-RPS19 antibodies are displayed below the corresponding gradient fractions.

(C) Overlay of the two polysome profiles shown in (A) and (B) for lymphoblastoid cells from a healthy control (ctl; dotted gray line) and from individual P2 (P2; solid black line).

4A and 4B). Importantly, we found that the RPL13 variant protein distributed in the gradient exactly as the wild-type protein. The variant is therefore incorporated into 60S subunits that form ribosomes competent for translation. We noticed, however, a decrease of the 80S and polysome peaks in the individual sample, which may indicate a change in translation dynamics (Figure 4C).

CD34+ cells isolated from peripheral blood were cultured in liquid culture over 15 days to evaluate erythroid proliferation. Only the late phase of the terminal erythroid differentiation was affected in the individual with the variant of *RPL13* (Figure S2A). Cell viability during the complete erythroid differentiation time course has been confirmed (Figure S2B).

To assess the localization pattern of RPL13 in bone growth plate, cross sections of growth plate from 8-week-old healthy male mice were analyzed through the use of immunohistochemistry. Immunostaining revealed that RPL13 is present in cells from the hypertrophic zone and the remodelling zone. A weaker immunostaining was observed in cells located in the bone marrow compartment (Figure 5). Subsequently, we also evaluated three different RPs from the large and the small subunits of the ribosomes. RPL3 (MIM: 604163), RPS3 (MIM: 600454), and RPS10 (MIM: 603632) were immunohistochemically detected in cells from the growth plate, and they displayed the same localization pattern as did RPL13. RPL3, RPS3, and RPS10 were also found in the bone marrow compartment (Figure 5).

In this study, we report four unrelated individuals with a severe bone dysplasia sharing common clinical and radiological features. The abnormalities shared by the four individuals confirm a rare form of SEMD previously described for two of them.[6] All individuals presented with short stature, genu varum, epimetaphyseal anomalies, and platyspondyly but did not show any other symptoms, nor did they show any hematological abnormality on blood counts. The decreased erythroid cell proliferation reported at the terminal orthochromatophilic erythroblast stage should not be sufficient to generate an erythroid blockade and a aregenerative anemia as seen in DBA.

All individuals harbored a *de novo RPL13* splice-site or missense variant. Based on the modeling of the adverse structural effects of the splice-site variants from two individuals, the mutant proteins are expected to be incorporated in pre-60S particles. Indeed, pre-rRNA processing does not seem to be affected in analyzed cells. We also showed that for variants c.477+1G>T and c.477+2 T>C, the variant protein is incorporated into the ribosomes to the same extent as is wild-type RPL13 in analyzed cells.

These data provide evidence that these de *novo* variants in *RPL13* cause a rare form of bone dysplasia with severe short stature, responsible for a human ribosomopathy which specifically affects bone tissue. Affected individuals

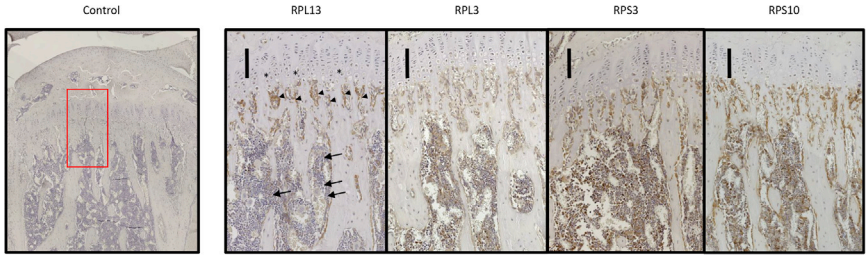

Figure 5. Immunochemistry of Four Riboproteins in Mouse Growth Plate

Micrographs of longitudinal sections of tibiae from 8-week-old mice immunohistochemically stained for the expression of RPL13, RPL3, RPS3, and RPS10. RPL13 is expressed in cells from the hypertrophic zone (black stars) and the remodeling zone (arrowheads) with a weaker staining in cells from the bone marrow compartment (solid arrows). Expression of RPL3, RPS3, and RPS10 was detected with the same pattern in the three compartments. Scale bars correspond to 100μm.

do not show any other symptoms such as anemia, bone marrow failure, or cranio-facial abnormalities, as can be observed in other ribosomopathies such as DBA, Shwachman-Diamond syndrome (SDS [MIM: 617941]) and cartilage hair hypoplasia (CHH-AD [MIM: 250250–607095]).[1]

RPL13, also known as eL13,[12] is a 211-amino-acid-long protein. RPL13 is known to be essential to ribosomal assembly because its depletion leads to maturation arrest at an early ribosomal assembly stage in yeast.[13] Consistently, we show that knockdown of RPL13 by siRNA in HeLa cells leads to an early defect in pre-rRNA processing, a defect which is characterized by an increase of the 45S and 41S precursors. However, our data suggest that ribosome biogenesis is not significantly affected by the variants reported here: we did not observe similar abnormality in pre-rRNA processing in the cells of individuals P1 and P2 (Figure 4B). We cannot exclude the possibility that a mild defect in ribosome biogenesis occurs in highly proliferative tissues like the growth plate, but could not be unambiguously detected here. The 60S subunits containing the RPL13 variants were detected in the same proportion as were the normal 60S subunits, including in the polysome fractions, which further indicates that incorporation of a variant RPL13 into a nascent 60S particle does not compromise its maturation, nor does it affect its stability in the cytoplasm. This is a fundamental difference compared to DBA, in which haploinsufficiency of RPs impairs synthesis of ribosomes and thereby decreases their production rate. The ribosomal profile on sucrose gradient in cells expressing the RPL13 variants is mildly changed, which suggests that translation is affected in individuals' cells. We assume that RPL13 could play a specific role in the translation of particular mRNAs in chondrocytes or/and osteoblasts of the growth plate. In support of this hypothesis, loss of function of RPs has already been linked to very specific developmental defects in mouse models in the absence of global translation defects.[14,15]

In DBA, mutations affecting RPs primarily affect erythropoiesis, but they also affect multiple other organs with variable penetrance. Skeletal abnormalities (e.g., abnormal thumbs, radial hypoplasia, short stature) have been reported in ribosomopathies such as DBA, but these conditions are not classified as skeletal dysplasias. In contrast, CHH-AD is a metaphyseal chondrodysplasia caused by *RMRP* (MIM: 157660) pathogenic variants and is considered to be a ribosomopathy.[16] *RMRP* is the RNA component of RNase MRP, a nucleolar ribonucleoprotein particle which catalyzes the endonucleolytic cleavage of the pre-rRNA at site 2.[17,18] *RMRP* is a key factor for the regulation of hypertrophic chondrocytes. It has been shown that the knockdown of *RMRP* leads to a defect of chondrocyte differentiation.[19] Our data show that RPL13, together with other RPs, is highly expressed in the growth plate and in cells lining the newly primary bone trabeculae, similar to RNase MRP. These high expression levels further stress the importance of ribosome biogenesis and translation in the growth plate. Whether the pathophysiological mechanisms underlying these two skeletal dysplasias share some common grounds remains to be explored.

Interestingly, a direct interaction between adenine 509 of the 28S rRNA and tyrosine 161 of RPL13 has been shown, with the adenine extruded from the double-stranded DNA.[20] Here, molecular modeling suggested that the 18-amino-acid insertion localized in this region might induce the removal of this interaction. A primary consequence of this insertion might be the blockade of a conserved 28S RNA binding on ES7L. Consistent with the production and stability of the 60S subunit containing the variants, the polypeptide insertion in RPL13 does not seem to influence the overall ribosome architecture. The p.Arg183Pro missense variant affects an amino acid which interacts with the 28S rRNA and is predicted to break the C-terminal alpha helix of RPL13, an alpha helix which extensively contacts the 28S rRNA. Hence, both splice and missense variants may destabilize the interaction of RPL13 C terminus with the 28S rRNA and compromise its function in translation.

In summary, our data demonstrate that *RPL13* variants cause a rare skeletal dysplasia with short stature. The identified *RPL13* variants do not modify overall ribosome biogenesis, even when the resulting variant RPL13 protein is integrated to the mature large subunit. This ribosomopathy might affect bone development by affecting the translation level of specific mRNAs in cells from the growth plate, as shown in the erythroid lineage. Future studies will attempt to unravel the specific impact of these *RPL13* variants on translation of key factors of the growth plate.

Accession Numbers

The ClinVar accession numbers for the newly reported sequence variants are VCV000689800, VCV000689801, VCV000689802, and VCV000689803 (GenBank: NM_000977.3).

Supplemental Data

Supplemental Data can be found online at https://doi.org/10.1016/j.ajhg.2019.09.024.

Acknowledgments

We would like to thank all families for participating in this study. P.E.G. and M.F.O'D. were funded by the Agence Nationale de la Recherche (ANR) grants ANR-15-CE12-0001 and ANR-16-CE11-0029 and by the European Research Area Network (ERA NET) E-RARE project and ANR grant ANR-15-RAR3-0007-04 (European Diamond-Blackfan Anemia Consortium [EuroDBA]).

Declaration of Interests

K.McW. is an employee of GeneDx. A.P. is an employee of Center for Genomics and Transcriptomics and Praxis für Humangenetik Tübingen. The other authors declare no competing interests.

Received: July 1, 2019
Accepted: September 20, 2019
Published: October 17, 2019

Web Resources

1000 Genomes, http://www.1000genomes.org/
Combined Annotation Dependent Depletion, https://cadd.gs.washington.edu
dbSNP, https://www.ncbi.nlm.nih.gov/projects/SNP/
Decipher, https://decipher.sanger.ac.uk/
ExAC Browser, http://exac.broadinstitute.org/
GenBank, https://www.ncbi.nlm.nih.gov/genbank/
Genematcher, https://genematcher.org/
GnomAD, https://gnomad.broadinstitute.org/
The Human Protein Atlas, http://www.proteinatlas.org/
MutationTaster, http://www.mutationtaster.org
NHLBI Exome Sequencing Project (ESP) Exome Variant Server, https://evs.gs.washington.edu/EVS/
OMIM, https://www.omim.org/
PLINK, https://pngu.mgh.harvard.edu/~purcell/plink/
PolyPhen-2, http://genetics.bwh.harvard.edu/pph2/
SIFT, http://sift.bii.a-star.edu.sg/
UCSC Genome Browser, http://genome.ucsc.edu

References

1. Trainor, P.A., and Merrill, A.E. (2014). Ribosome biogenesis in skeletal development and the pathogenesis of skeletal disorders. Biochim. Biophys. Acta *1842*, 769–778.
2. Aubert, M., O'Donohue, M.F., Lebaron, S., and Gleizes, P.E. (2018). Pre-Ribosomal RNA Processing in Human Cells: From Mechanisms to Congenital Diseases. Biomolecules *8*, E123.
3. Bolze, A., Boisson, B., Bosch, B., Antipenko, A., Bouaziz, M., Sackstein, P., Chaker-Margot, M., Barlogis, V., Briggs, T., Colino, E., et al. (2018). Incomplete penetrance for isolated congenital asplenia in humans with mutations in translated and untranslated *RPSA* exons. Proc. Natl. Acad. Sci. USA *115*, E8007–E8016.
4. Paolini, N.A., Attwood, M., Sondalle, S.B., Vieira, C.M.D.S., van Adrichem, A.M., di Summa, F.M., O'Donohue, M.F., Gleizes, P.E., Rachuri, S., Briggs, J.W., et al. (2017). A Ribosomopathy Reveals Decoding Defective Ribosomes Driving Human Dysmorphism. Am. J. Hum. Genet. *100*, 506–522.
5. Nieminen, T.T., O'Donohue, M.F., Wu, Y., Lohi, H., Scherer, S.W., Paterson, A.D., Ellonen, P., Abdel-Rahman, W.M., Valo, S., Mecklin, J.P., et al. (2014). Germline mutation of RPS20, encoding a ribosomal protein, causes predisposition to hereditary nonpolyposis colorectal carcinoma without DNA mismatch repair deficiency. Gastroenterology *147*, 595–598.e5.
6. Isidor, B., Geffroy, L., de Courtivron, B., Le Caignec, C., Thiel, C.T., Mortier, G., Cormier-Daire, V., David, A., and Toutain, A. (2013). A new form of severe spondyloepimetaphyseal dysplasia: clinical and radiological characterization. Am. J. Med. Genet. A. *161A*, 2645–2651.
7. Sobreira, N., Schiettecatte, F., Valle, D., and Hamosh, A. (2015). GeneMatcher: a matching tool for connecting investigators with an interest in the same gene. Hum. Mutat. *36*, 928–930.
8. Schwarz, J.M., Rödelsperger, C., Schuelke, M., and Seelow, D. (2010). MutationTaster evaluates disease-causing potential of sequence alterations. Nat. Methods *7*, 575–576.
9. Adzhubei, I.A., Schmidt, S., Peshkin, L., Ramensky, V.E., Gerasimova, A., Bork, P., Kondrashov, A.S., and Sunyaev, S.R. (2010). A method and server for predicting damaging missense mutations. Nature Methods *7*, 248–249.
10. Kircher, M., Witten, D.M., Jain, P., O'Roak, B.J., Cooper, G.M., and Shendure, J. (2014). A general framework for estimating the relative pathogenicity of human genetic variants. Nat. Genet. *46*, 310–315.
11. Xu, J., and Zhang, Y. (2010). How significant is a protein structure similarity with TM-score = 0.5? Bioinformatics *26*, 889–895.
12. Ban, N., Beckmann, R., Cate, J.H., Dinman, J.D., Dragon, F., Ellis, S.R., Lafontaine, D.L., Lindahl, L., Liljas, A., Lipton, J.M., et al. (2014). A new system for naming ribosomal proteins. Curr. Opin. Struct. Biol. *24*, 165–169.
13. Gamalinda, M., Ohmayer, U., Jakovljevic, J., Kumcuoglu, B., Woolford, J., Mbom, B., Lin, L., and Woolford, J.L., Jr. (2014). A hierarchical model for assembly of eukaryotic 60S ribosomal subunit domains. Genes & development *28*, 198–210.
14. Kondrashov, N., Pusic, A., Stumpf, C.R., Shimizu, K., Hsieh, A.C., Ishijima, J., Shiroishi, T., and Barna, M. (2011). Ribosome-mediated specificity in Hox mRNA translation and vertebrate tissue patterning. Cell *145*, 383–397.
15. Anderson, S.J., Lauritsen, J.P., Hartman, M.G., Foushee, A.M., Lefebvre, J.M., Shinton, S.A., Gerhardt, B., Hardy, R.R., Oravecz, T., and Wiest, D.L. (2007). Ablation of ribosomal protein L22 selectively impairs alphabeta T cell development by activation of a p53-dependent checkpoint. Immunity *26*, 759–772.
16. Mattijssen, S., Welting, T.J., and Pruijn, G.J. (2010). RNase MRP and disease. Wiley Interdiscip. Rev. RNA *1*, 102–116.
17. Gill, T., Cai, T., Aulds, J., Wierzbicki, S., and Schmitt, M.E. (2004). RNase MRP cleaves the CLB2 mRNA to promote cell cycle progression: novel method of mRNA degradation. Mol. Cell. Biol. *24*, 945–953.
18. Goldfarb, K.C., and Cech, T.R. (2017). Targeted CRISPR disruption reveals a role for RNase MRP RNA in human preribosomal RNA processing. Genes & development *31*, 59–71.
19. Steinbusch, M.M.F., Caron, M.M.J., Surtel, D.A.M., Friedrich, F., Lausch, E., Pruijn, G.J.M., Verhesen, W., Schroen, B.L.M., van Rhijn, L.W., Zabel, B., and Welting, T.J.M. (2017). Expression of RMRP RNA is regulated in chondrocyte hypertrophy and determines chondrogenic differentiation. Sci. Rep. *7*, 6440.
20. Anger, A.M., Armache, J.P., Berninghausen, O., Habeck, M., Subklewe, M., Wilson, D.N., and Beckmann, R. (2013). Structures of the human and Drosophila 80S ribosome. Nature *497*, 80–85.

The American Journal of Human Genetics, Volume *105*

Supplemental Data

RPL13 Variants Cause Spondyloepimetaphyseal Dysplasia with Severe Short Stature

Cedric Le Caignec, Benjamin Ory, François Lamoureux, Marie-Francoise O'Donohue, Emilien Orgebin, Pierre Lindenbaum, Stéphane Téletchéa, Manon Saby, Anna Hurst, Katherine Nelson, Shawn R. Gilbert, Yael Wilnai, Leonid Zeitlin, Eitan Segev, Robel Tesfaye, Mathilde Nizon, Benjamin Cogne, Stéphane Bezieau, Loic Geoffroy, Antoine Hamel, Emmanuelle Mayrargue, Benoît de Courtivron, Aliette Decock-Giraudaud, Céline Charrier, Olivier Pichon, Christelle Retière, Richard Redon, Alexander Pepler, Kirsty McWalter, Lydie Da Costa, Annick Toutain, Pierre-Emmanuel Gleizes, Marc Baud'huin, and Bertrand Isidor

Figure S1

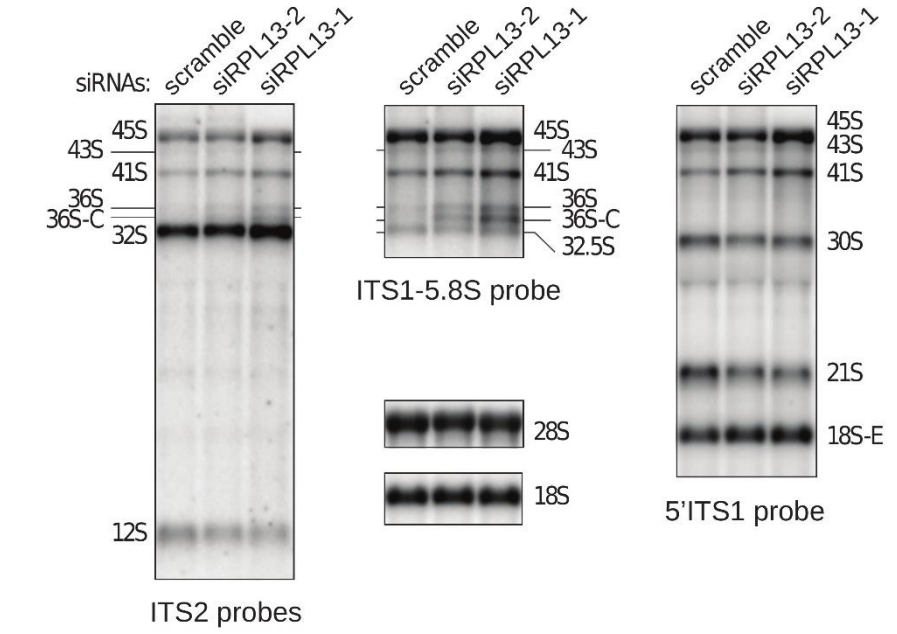
siRNAs:
scramble
siRPL13-2
siRPL13-1
45S
43S
41S
36S
36S-C
32S
12S
ITS2 probes
32.5S
ITS1-5.8S probe
28S
18S
30S
21S
18S-E
5'ITS1 probe

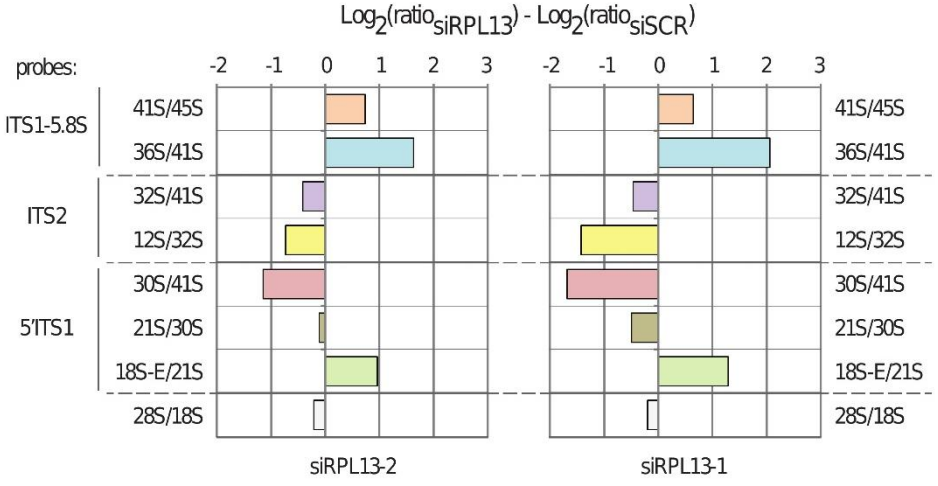
Log2(ratio siRPL13) - Log2(ratio siSCR)
probes:
-2
-1
0
1
2
3
ITS1-5.8S
ITS2
5'ITS1
41S/45S
36S/41S
32S/41S
12S/32S
30S/41S
21S/30S
18S-E/21S
28S/18S
siRPL13-2
siRPL13-1

Figure S2

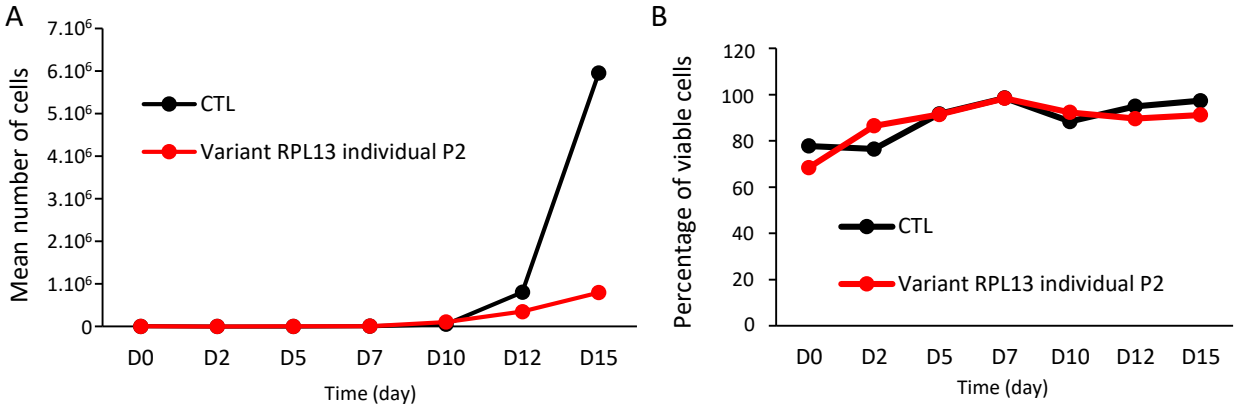
A
Mean number of cells
7.10⁶
6.10⁶
5.10⁶
4.10⁶
3.10⁶
2.10⁶
1.10⁶
0
CTL
Variant RPL13 individual P2
D0
D2
D5
D7
D10
D12
D15
Time (day)
B
Percentage of viable cells
120
100
80
60
40
20
0
CTL
Variant RPL13 individual P2
D0
D2
D5
D7
D10
D12
D15
Time (day)

SUPPLEMENTAL FIGURE LEGENDS

Figure S1. Consequence of mutant RPL13 on pre-rRNA processing.

Northern blot analysis of pre-RNAs in lymphoblastoid cells treated with siRNAs targeting RPL13 mRNAs. The 5'ITS1 and the ITS2 probes detect the precursors to the 40S and 60S subunit RNAs, respectively. The ITS1-5.8S probe evidences an accumulation of 36S and 36S-C precursors when the level of RPL13 is reduced, which is indicative of a defect in cleavage at site 2. This cleavage occurs early and produces two separate pathways for the small and large ribosomal precursors.

Figure S2 : Erythroid proliferation is decreased in the variant RPL13 individual compared to the healthy control.

(A) Mean erythroid progenitor cell proliferation and (B) cell viability of peripheral $CD34^{+}$ cells from the variant RPL13 individual and from the control, from D0 to D15 during the complete erythroid differentiation (Mean of technical triplicates).

Table S1 : Primers for RPL13 RT-PCR

	Forward	Reverse
RPL13 (NM_000977.3)	ATGGCGCCCAGCCGGAATGG	AAACACACCACGTGGAGACC

MATERIALS AND METHODS

Individuals and Exome sequencing

Exome sequencing was performed in individuals P1, P2 and their parents following previously described procedures[1]. Through GeneMatcher[2], we subsequently identified two additional individuals (P3 and P4), yielding a total of four affected subjects from four families. All variants were confirmed by Sanger sequencing. We obtained written informed consent from all study participants in accordance with a protocol approved by respective institutional review boards (Nantes CHU ethical committee (MESR DC-2017-2987))

Fastqs of 60 samples (P1, P2, their parents and 54 samples unrelated to the present study) were mapped to grch37 using bwa-mem 0.7.12 and called with GATK 3.7.0 according to the Broad-Institute best-practices but the variants were not recalibrated because there were not enough data. The resulting VCF was annotated with SnpEff 4.3 and the gnomad database. De-novo genotypes called in either P1 and P2 but absent for the other individuals, missing in gnomad, were selected using vcffilterjs and grouped by gene using jvarkit/groupbygene. The candidate variants were visually checked with IGV.

The coding regions and flanking intronic regions of individual P3 and its parents were enriched using Agilent SureSelect XT All Exon V7 in-solution technology and were sequenced using the Illumina NovaSeq system. Illumina bcl2fastq2 was used to demultiplex sequencing reads. The reads were mapped to the human reference genome (hg19) using the Burrows Wheeler Aligner, and variants were called using Samtools and Varscan. Variants in the coding region and the flanking intronic regions (±8 bp) with a minor allele frequency (MAF) < 1.5% were evaluated. Known disease-causing variants (according to HGMD) within ±30 bp of flanking regions and up to 5% MAF were also evaluated. MAFs were taken from gnomAD and an in-house database. NGS based CNV calling was computed using an internally-developed method based on sequencing coverage depth; a model of the expected coverage that represents wet-lab biases as

well as inter-sample variation was used. CNV calling was performed by computing the sample's normalized coverage profile and its deviation from the expected coverage. Variants found in patient P3 and in its parents were compared and filtered for four cases: *de novo* in the patient, patient is compound heterozygous, patient is homozygous and the parents are heterozygous, patient is hemizygous and the mother is heterozygous for variants on the X-chromosome. Variants were evaluated based on the ACMG guidelines for the interpretation of sequence variants. Several additional in-silico panels were used to exclude the possible presence of non-trio variants which could explain the phenotype of the patient.

Using genomic DNA from individual P4 and parents, the exonic regions and flanking splice junctions of the genome were captured using the IDT xGen Exome Research Panel v1.0. Massively parallel (NextGen) sequencing was done on an Illumina system with 100bp or greater paired-end reads. Reads were aligned to human genome build GRCh37/UCSC hg19, and analyzed for sequence variants using a custom-developed analysis tool. Additional sequencing technology and variant interpretation protocol has been previously described [3]. The general assertion criteria for variant classification are publicly available on the GeneDx ClinVar submission page http://www.ncbi.nlm.nih.gov/clinvar/submitters/26957/

Reverse transcription–PCR.

Total RNA was extracted from peripheral blood cells (P1 and P2), using TriReagent (Life Technologies). Total RNA was reversed transcribed using the ThermoScript RT–PCR System (Life Technologies). Two microliters of the RT reaction were subjected to Polymerase Chain Reaction (Life Technologies) using 0.2 µM of forward and reverse primers (Table S1). PCR were carried for 30 cycles. Each cycle consisted of 1 minute of denaturation at 94°C, 1 minute of annealing at 62°C and 1 minute of extension at 72°C. PCR products were were separated in a 1,7% agarose/1x TAE gel at 120 V for 1 hour and stained with SybrSafe (Life Technologies).

Pictures of the gel were taken by CCD camera under UV light (Syngene) and are representative of 3 independent experiments.

Western blotting analysis

Lymphoblastoid cells were established by EBV transformation of peripheral B cells using EBV supernatant harvested from the cell line B95-8 (American Type Culture Collection). Mesenchymal stem cells (P1 and healthy donor) and lymphoblastoid cells (P2 and healthy donor) were cultured respectively α-MEM and RPMI (GIBCO). Healthy donor cells were not matched for age and sex with individuals P1 and P2 cells. After cells lysis, samples containing equal amounts of protein (50 µg) were separated on 16% SDS-polyacrylamide gels, and proteins were transferred to polyvinylidene difluoride membranes. The membranes were blocked in blocking buffer (LiCor, USA) at room temperature for 1 hour and blots were probed overnight at 4 °C with primary antibodies (RPL13, 1:800; Sigma-Aldrich) or vinculin (1:10.000; Cell signaling) to detect proteins of interests. After incubation, the membranes were washed three times with washing buffer (PBS containing 0.1% Tween) for 5 minutes. Membranes were then incubated for 1 hour with 1:10,000 diluted secondary antibodies (Li-Cor) at room temperature. Specific proteins were detected using Odyssey Fc (Li-Cor) after washing. Pictures are representative of 3 independent experiments.

Structural modelling

The protein structure of the mutated RPL13 protein was predicted using I-TASSER 5.1 [4-6]. I-TASSER selected the structure of the human ribosome as the best template (4V6X, [7]) to build high quality models. Visual inspection of models and interaction analysis were done with PyMOL 1.8 [8].

Tissue culture and siRNA treatment

HeLa cells were cultured in DMEM (GIBCO) supplemented with 10% fetal bovine serum and 1 mM sodium pyruvate (Sigma). Two 21-mer siRNA duplexes (Eurogentec) were used to knock down expression of the human RPL13 mRNAs in HeLa cells (siRPL13-1: 5'-GGAAGAGAAGAAUUUCAAAdTdT-3'; siRPL13-2: 5'-CGUCUAUAAGAAGGAGAAAdTdT-3'). Knockdown efficiency was verified by qPCR. Each siRNA solution was added at a final concentration of 500 nM to 200 ml of cell suspension (50.10^6 cells/ml diluted in Na phosphate buffer, pH 7.25, containing 250 mM sucrose and 1 mM MgCl2). Electro-transformation was performed at 240 V with a Gene Pulser (Bio-Rad)[9]. Control HeLa cells were electro-transformed with a scramble siRNA (siRNA-negative control duplex; Eurogentec). After 10 minutes of incubation at ambient temperature, cells were plated and grown at 37°C for 48 hours.

RNA extraction and analysis by northern blot

Total RNAs were extracted with TriReagent from cell pellets containing $20\text{-}30.10^6$ cells. The aqueous phase was further extracted with phenol-chloroform-isoamylic alcohol (25:24:1; Sigma), then with chloroform. Total RNAs were recovered after precipitation with 2-propanol. For Northern blot analyses, RNAs were dissolved in formamide, denatured for 10 minutes at 70°C, and separated on a 1.2% agarose gel containing 1.2% formaldehyde and 1X Tri/Tri buffer (30 mM triethanolamine, 30 mM tricine, pH 7.9) (3 µg RNAs/lane). RNAs were transferred to a Hybond N^+ nylon membrane (GE Healthcare) by passive transfer and cross-linked under UV light. Pre-hybridization was performed for 1 hour at 45°C in 6X SSC, 5X Denhardt's solution, 0.5% SDS, 0.9 g/ml tRNA. The 5'-radiolabeled oligonucleotide probe was incubated overnight. The sequences of the probes were: 5'-ITS1 (50-CCTCGCCCTCCGGGCTCCGTTAATGATC-

3'), ITS1-5.8S (5'-CTAAGAGTCGTACGAGGTCG-3'), ITS2 (ITS2b: 5'-CTGCGAGGGAACCCCCAGCCGCGCA-3' and ITS2d/e: 5'-GCGCGACGGCGGACGACACCGCGGCGTC-3'), 18S (5'-TTTACTTCCTCTAGATAGTCAAGTTCGACC-3'), 28S (5'-CCCGTTCCCTTGGCTGTGGTTTCGCTAGATA-3'). Membranes were washed twice for 10 minutes in 2X SSC, 0.1% SDS and once in 1X SSC, 0.1% SDS, and then exposed. Signals were acquired with a Typhoon Trio PhosphorImager (GE Healthcare) and quantified using the MultiGauge software. Pictures are representative of 3 independent experiments.

Polysome profiling

Lymphoblastoid cells (healthy donors and individual 2) were treated with 100 µg/ml cycloheximide (Sigma-Aldrich) for 10 min. The cytoplasmic fractions were prepared on ice as described above, except that cycloheximide was added to all buffers [10]. A sample volume containing 1 mg of total proteins was loaded on a 10–50% (wt/wt) sucrose gradient and the tubes were centrifuged at 36 000 rpm and at 4°C for 2 hours in a SW41 rotor (Optima L100XP ultracentrifuge; Beckman Coulter). The gradient fractions were collected at OD254 nm with a Foxy Jr. gradient collector (Teledyne Isco). Each fraction was centrifuged on a Vivaspin 500 concentrator (Sartotrius Stedim Biotech) in order to remove sucrose. Half of it was then used for RNA extraction with TriReagent, while the other half was used to extract total proteins with TCA.

Culture of human primary cells

CD34+ cells from peripheral blood of individual P2 and a healthy control were isolated by immunomagnetic technique using manual column (Miltenyi Biotec, Paris, France). Purified CD34+ cells were cultured in IMDM medium using 3% AB serum (Sigma Aldrich), 2% human peripheral blood plasma (stem cell technologies), 10 µg/ml Insulin (Sigma Aldrich), 3U/ml

Heparin (Sigma Aldrich), 200 µg/ml Holo-Transferrin (Sigma Aldrich), 10 ng/ml stem cell factor (SCF) (Miltenyl biotech), 1 ng/ml IL3 (Stem Cell Technologies), 3 IU/ml EPO and 1% Penicillin/Streptomycin (final concentrations). This media was used from day 0 to day 6, then deprivated from IL3 and EPO concentration was used at 1 IU/ml from day 7 to day 10. From day 11 to day 15, SCF was removed and EPO and Holo-Transferrin was used respectively at 0.1 IU/ml and 1 mg/ml, and 100% Penicillin/Streptomycin (final concentrations). Viable cells were counted in triplicate using the trypan blue dye exclusion test as a function of time in culture. Bars represent mean of technical triplicate.

Immunochemistry

All procedures involving mice (their housing and care in the Experimental Therapeutic Unit at the Faculty of Medicine of Nantes, France, the method by which they were anesthetized and killed, and all experimental protocols) were conducted in accordance with the institutional guidelines of the French Ethical Committee (CEEA.PdL.2011.32). Eight-week old C57BL/6 male mice were sacrificed, tibiae were collected and were decalcified with 4.13% EDTA and 0.2% paraformaldehyde in phosphate buffered saline (PBS) for 96 hours using the KOS microwave histostation (Milestone, Kalamazoo, MI) before embedding in paraffin. Sections (3 µm thick, Leica Microsystems) were analyzed by immunostaining for RPL13, RPL3, RPS3 and RPS10. Protocols were performed as described previously [11] with rabbit anti-RPL13, anti-RPL3, anti-RPS3 and anti-RPS10 antibodies (1/800; Sigma for RPL13 and 1/1000 GeneTex for RPL3, RPS3 and RPS10).

REFERENCES OF SUPPLEMENTAL DATA

1. Isidor, B., Lindenbaum, P., Pichon, O., Bezieau, S., Dina, C., Jacquemont, S., Martin-Coignard, D., Thauvin-Robinet, C., Le Merrer, M., Mandel, J.L., et al. (2011). Truncating mutations in the last exon of NOTCH2 cause a rare skeletal disorder with osteoporosis. Nature genetics 43, 306-308.
2. Sobreira, N., Schiettecatte, F., Valle, D., and Hamosh, A. (2015). GeneMatcher: a matching tool for connecting investigators with an interest in the same gene. Hum Mutat 36, 928-930.
3. Retterer, K., Juusola, J., Cho, M.T., Vitazka, P., Millan, F., Gibellini, F., Vertino-Bell, A., Smaoui, N., Neidich, J., Monaghan, K.G., et al. (2016). Clinical application of whole-exome sequencing across clinical indications. Genet Med 18, 696-704.
4. Roy, A., Kucukural, A., and Zhang, Y. (2010). I-TASSER: a unified platform for automated protein structure and function prediction. Nature protocols 5, 725-738.
5. Yang, J., Yan, R., Roy, A., Xu, D., Poisson, J., and Zhang, Y. (2015). The I-TASSER Suite: protein structure and function prediction. Nature methods 12, 7-8.
6. Zhang, Y. (2008). I-TASSER server for protein 3D structure prediction. BMC bioinformatics 9, 40.
7. Anger, A.M., Armache, J.P., Berninghausen, O., Habeck, M., Subklewe, M., Wilson, D.N., and Beckmann, R. (2013). Structures of the human and Drosophila 80S ribosome. Nature 497, 80-85.
8. Schrödinger, L. (2015). The PyMOL Molecular Graphics System, Version 1.8.
9. Paganin-Gioanni, A., Bellard, E., Escoffre, J.M., Rols, M.P., Teissie, J., and Golzio, M. (2011). Direct visualization at the single-cell level of siRNA electrotransfer into cancer cells. Proceedings of the National Academy of Sciences of the United States of America 108, 10443-10447.
10. Baudin-Baillieu, A., Hatin, I., Legendre, R., and Namy, O. (2016). Translation Analysis at the Genome Scale by Ribosome Profiling. Methods Mol Biol 1361, 105-124.
11. Baud'huin, M., Lamoureux, F., Jacques, C., Rodriguez Calleja, L., Quillard, T., Charrier, C., Amiaud, J., Berreur, M., Brounais-LeRoyer, B., Owen, R., et al. (2017). Inhibition of BET proteins and epigenetic signaling as a potential treatment for osteoporosis. Bone 94, 10-21.